JOURNAL OF PROPULSION AND POWER
Vol. 12, No. 3, May–June 1996

Examination of Chemical Approaches to Stabilizing Composite-Propellant Combustion

Merrill K. King*
Universities Space Research Association, Washington, D.C. 20024

Acoustic-mode combustion instability has long plagued the solid-propellant industry, and increased requirements for reduced-smoke propellants, with the elimination of metal oxide particulate products that damp acoustic oscillations, is expected to exacerbate this problem. One strategy for alleviating the problem involves identifying approaches to decrease a major source of acoustic energy, the transient burning-rate response of the propellant to pressure oscillations. In this study, a model was developed and used to define potential effects of varying either oxidizer or fuel ablation activation energy on the pressure-coupled response function. Based on calculations with unimodal-oxidizer-size formulations, it appears that increasing oxidizer ablation activation energy at a fixed value of binder ablation activation energy or increasing binder ablation activation energy at fixed oxidizer ablation activation energy can result in a significant reduction of this pressure-coupled burning rate response.

Nomenclature

A = $f_1(\bar{T}_s - T_0)$
AFU = fuel (binder) surface area
$ASOX$ = oxidizer surface area
A_1 = pre-exponential for oxidizer ablation rate expression
A_2 = pre-exponential for fuel ablation rate expression
c_{ps} = propellant specific heat
D_{ox} = oxidizer particle diameter
E_{fuel} = fuel ablation activation energy
E_{ox} = oxidizer ablation activation energy
f = oscillation frequency
f_1 = $(m_s'/\bar{m}_s)/T_s'$
f_3 = see Eq. (22)
f_4 = $3600f_3 - (dQ_{surf}/dT_s)$
H_{packet} = enthalpy per unit mass of packet of fuel plus oxidizer gas
j = $\sqrt{-1}$
K_g = gas thermal conductivity
K_s = solid thermal conductivity
L = defined by Eq. (15)
M = defined by Eq. (17)
m, m_s = mass burning flux
N = defined by Eq. (16)
OF_{packet} = oxidizer/fuel ratio of packet of gases leaving surface
OF_{prop} = overall propellant oxidizer/fuel ratio
P = pressure
Q_{gas} = gas-phase heat release per unit mass
Q_{surf} = net heat release in surface processes per unit mass
q_{fdbk} = heat-feedback flux from gas flame to surface
R = gas-law constant
R_{pc} = pressure-coupled response function
r = linear regression rate of propellant
S_f = fuel surface area
S_{ox} = oxidizer surface area
T_f = flame temperature
$TIMRAT$ = ratio of oscillation time to characteristic burning time, Eq. (29)
T_s = surface temperature
T_0 = propellant bulk (conditioning) temperature
WFO = weight fraction oxidizer in propellant
X = axial distance from surface into propellant
β = $-\bar{Q}_{surf}/(\bar{T}_s - T_0)$
ΔH_{TOT} = total available energy associated with a packet of gas leaving surface
λ = complex function of oscillation frequency, Eq. (7)
ρ_{prop} = propellant density
ω = angular frequency of oscillations, $2\pi f$
ω_p = dimensionless angular frequency of oscillations, Eq. (8)

Superscripts
$'$ = perturbation quantity
$-$ = steady-state (mean) quantity

Received June 16, 1994; revision received June 5, 1995; accepted for publication Sept. 22, 1995.

*Senior Scientist; currently on IPA assignment to Code UGS, NASA Headquarters, 300 E Street, SW, Washington, DC 20546. Associate Fellow AIAA.

Introduction

COMBUSTION instabilities in solid rocket motors have cost hundreds of millions of dollars in development and refurbishment costs as well as leading to performance compromises associated with fixes to these instabilities. Before 1960, instabilities occurred quite frequently in solid motors, particularly tactical motors where natural resonant frequencies are typically in the 1 kHz and higher regime. A fortuitous fix to many of these instabilities was found to be introducing large amounts of metal additives to the propellants, with the resulting condensed-phase products producing major damping of oscillations.

However, increasingly stringent mission requirements have led to increased incidence of instabilities in modern rocket motors, even with large amounts of metal additive. In addition, requirements for reduced-smoke propellants for tactical missiles, precluding inclusion of more than minor amounts of metal particles, have led to a considerable increase in the occurrence of instabilities. Accordingly, it is important that an alternative approach to alleviating the instability problems, namely, reduction of acoustic-energy source terms, be addressed; a major source term results from interaction of an acoustic wave with solid-propellant combustion processes. Both pressure and flow oscillations associated with an acoustic wave can cause burning rate oscillations that, in turn, feed energy into the acoustic wave. Attention here is restricted to

the pressure-coupled response function. The real part of this complex function is the important quantity for acoustic driving; relationships between the growth constant for oscillations and the pressure-coupled response function are discussed in Ref. 1. Developing means of reducing pressure-coupled response functions can result in a major reduction of instability problems in motors.

For many years, analysts have estimated pressure-coupled response functions for composite propellants using theoretical approaches equivalent to the well-known Zeldovich–Novozhilov approach,[2] but with limiting restrictions strictly applicable only to homogeneous propellants. As shown by King[3–5] (utilizing simplified composite propellant combustion models), composite propellants provide an additional coupling mechanism not treated by these approaches. This mechanism involves oscillations in the oxidizer/fuel ratio of packets of gases leaving the surface of the propellant (and in gas-phase heat release). These occur in conjunction with oscillations in surface temperature because of different activation energies for the fuel and oxidizer ablation processes. [See Ref. 5 for a discussion of how this invalidates the $q' = (\partial\bar{q}/\partial\bar{m})_{\bar{p}}m' + (\partial\bar{q}/\partial\bar{P})_{\bar{m}}P'$ relationship invoked (implicitly or explicitly) in the homogeneous propellant ZN approaches.]

The oxidizer/fuel ratio of each packet of gas leaving the propellant surface may be calculated as

$$OF_{\text{packet}} = A_1 \exp(-E_{\text{ox}}/RT_s)S_{\text{ox}}/A_2 \exp(-E_{\text{fuel}}/RT_s)S_f \quad (1)$$

At steady state, overall continuity forces these surface areas to adjust such that OF is equal to the overall propellant oxidizer/fuel ratio:

$$\bar{S}_{\text{ox}}/\bar{S}_f = OF_{\text{prop}}[A_2 \exp(-E_{\text{fuel}}/R\bar{T}_s)/A_1 \exp(-E_{\text{ox}}/R\bar{T}_s)] \quad (2)$$

If under oscillatory conditions the frequency is sufficiently high that S_{ox} and S_f cannot adjust away from steady-state values, it may be shown by combining Eqs. (1) and (2) (linearizing around $\bar{T}_s$) that

$$OF_{\text{packet}} = OF_{\text{prop}} \exp[(E_{\text{ox}} - E_{\text{fuel}})(T_s - \bar{T}_s)/R\bar{T}_s^2] \quad (3)$$

(In actuality there will be oscillations in surface structure partially compensating for the differential temperature sensitivities of fuel and oxidizer ablation, the degree of compensation increasing with decreasing oscillation frequency.) For a typical AP/HTPB composite propellant, available chemical enthalpy is related to the O/F ratio approximately by

$$H_{\text{packet}} = 800 + 180(OF_{\text{packet}} - 3.87) \quad (4)$$

leading to

$$H_{\text{packet}} = 800 + 180\{OF_{\text{prop}} \exp[(E_{\text{ox}} - E_{\text{fuel}}) \times (T_s - \bar{T}_s)/R\bar{T}_s^2] - 3.87\} \quad (5)$$

Since the ablation of ammonium perchlorate has a somewhat higher activation energy than the ablation of typical HTPB binders (by approximately 5 kcal/mole), upward perturbations in surface temperature will be accompanied by similar upward perturbations in packet oxidizer/fuel ratio, in turn leading to increases in gas-phase heat release with increases in surface temperature, a destabilizing mechanism.

In the work described in Ref. 5, Eq. (5) was combined with a simplified gas-phase combustion model, a full-up perturbation analysis of the equation set describing surface and gas-phase processes, and a Fourier analysis of the subsurface region for development of expressions relating the real part of the pressure-coupled response function $[R_{\text{pc}}^{(\text{real})} \equiv (m_s'/\bar{m})/(P'/\bar{P})]$, to the dimensionless angular frequency of oscillations at several values of $E_{\text{ox}} - E_{\text{fuel}}$. As Fig. 1 shows, the differential

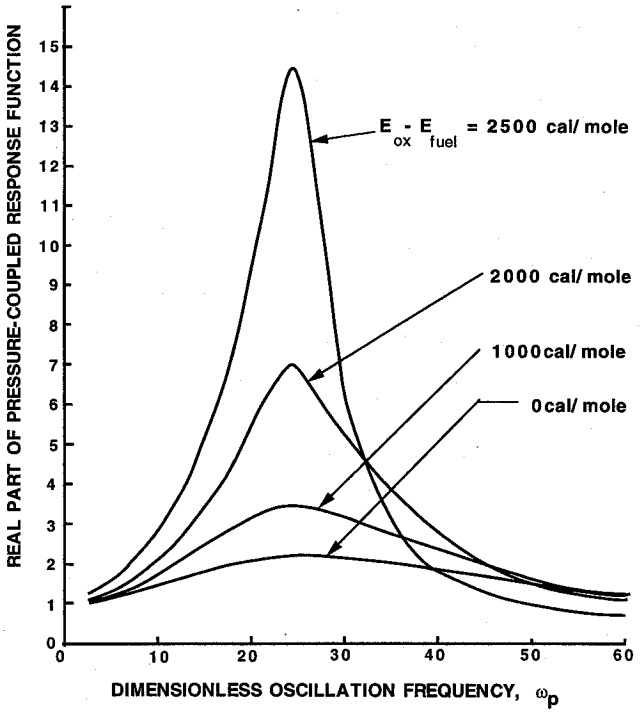

Fig. 1 Effects of allowance for dependence of O/F ratio of gases leaving surface on surface temperature; preliminary model.

dependence of oxidizer and fuel ablation rates was predicted to have a significant effect, with the predicted $R_{\text{pc}}^{(\text{real})}$ peak increasing dramatically with increasing values of $E_{\text{ox}} - E_{\text{fuel}}$. Thus, a potential destabilizing mechanism in AP-composite propellant combustion not present with homogeneous propellants is suggested. More important, this reasoning suggests that increasing the temperature sensitivity of fuel ablation or decreasing that of oxidizer ablation may lead to AP propellants with improved stability.

The current study was directed at further examination of this approach through development of a model based on perturbation analysis of a complex steady-state composite propellant combustion model to quantitate potential effects of altering oxidizer or fuel ablation activation energies.

Steady-State Model Utilized

A complex steady-state model of combustion of composite solid propellants developed by King[6–9] in the late 1970s was selected as a starting point. This model, based on the same principles as the Beckstead–Derr–Price (BDP) model,[10] but with several major modifications, was first further modified to eliminate a discrepancy present in most BDP-type models. [In these models, relative surface areas of the oxidizer and fuel are calculated via geometrical considerations, with the ratio of surface area of the fuel to planar oxidizer surface area being assumed to be equal to the volumetric ratio of fuel-to-oxidizer; as a result, since volumetric ablation rates of the fuel and oxidizer are in general different, mass is not conserved. This deficiency has been corrected in the steady-state model used here through an iterative approach (described later) to the calculation of fuel surface area associated with a given oxidizer particle planar surface area to ensure that the ratio of products of areas and mass fluxes of oxidizer and fuel is equal to the mass ratio of these ingredients in the propellant.] Details of the equation development for this model appear in Refs. 6 and 7. Extension of the model to treat multimodal-oxidizer formulations and metallized AP/HTPB formulations are discussed in Refs. 7–9.

The only aspect of the current steady-state model not discussed in those references involves the modification made to ensure the conservation of mass through adjustment of the fuel

area associated with each oxidizer particle. In the first loop of a trial-and-error procedure, this fuel surface area is calculated by equating the ratio of fuel surface area to oxidizer planar-projection surface area to the volumetric ratio of these ingredients in the formulation (as in earlier models); in subsequent loops, the ratio of {oxidizer mass flux times oxidizer surface area divided by fuel mass flux times fuel area} to {overall oxidizer/fuel ratio} is calculated: if this ratio is greater than unity, the value of fuel area is raised, whereas if it is less than unity, it is lowered for the next calculation loop. This looping procedure is continued until the ratio crosses unity with a Newton–Raphson procedure then being employed to final convergence.

As indicated in Refs. 6–9, there are three free constants, associated with chemical kinetic expressions, included in the model described previously; optimized values for these constants were chosen by calibration against burning rate vs pressure data for four unimodal-oxidizer-size AP/HTPB formulations (three 73-wt% AP formulations with oxidizer diameters of 5, 20, and 200 μm and one 77-wt% AP formulation with 20-μm-diam particles). Predictions and data were found to agree quite well, except for the 200-μm AP formulation, where predicted values ranged from 5% high at 10 atm to 40% high at 150 atm. Similar comparisons were also made of predicted and experimental burning rates vs pressure for five 82-wt% AP multimodal particle size formulations (four bimodal and one trimodal), with no further adjustment of the constants; agreement between predictions and data was excellent for all formulations except a fifty–fifty 20/200-μm bimodal AP formulation, where predictions were approximately 10% high. Thus, it appears that this steady-state model used as a basis for the unsteady-state burning rate studies described in the remainder of this article is a reasonable representation of AP/HTPB composite propellant combustion. One point that should be noted, however, is that this model employs a single-surface-temperature approximation. One could relax this approximation to allow for different surface temperatures for oxidizer and fuel; this would lead to a large increase in complexity of the following unsteady-state analysis, but might be worth pursuing.

Unsteady-State Modeling

A description is presented of a perturbation analysis of this steady-state model, with a Fourier analysis of the propellant subsurface region plus a quasi-steady-state analysis of surface and gas-phase processes including allowance for perturbations in gas-phase oxidizer/fuel ratio. Effects of partial adjustments of oxidizer and fuel areas to oscillations in ablation fluxes were treated parametrically; estimates of the degree of surface areas adjustment were based on the ratio of the oscillation period to the time required for burning of a propellant thickness equal to the oxidizer diameter.

The analysis of the response of the subsurface regions to oscillations in heat feedback flux is a standard one (described in detail in Ref. 3), resulting in the following relationship of the perturbation values of temperature gradient just below the surface, surface temperature, and burning rate:

$$\left[\frac{K_s\,\partial T'}{\partial X}\right]_{s^-} = \rho_P \bar{r} c_{p,s}\left\{\lambda T_s' + \left[\frac{(\bar{T}_s - T_0)}{\lambda}\right]\left(\frac{r'}{\bar{r}}\right)\right\} \tag{6}$$

where λ is given by

$$\lambda^2 - \lambda - j\omega_p/4 = 0 \tag{7}$$

$$\omega_p = 4K_s\rho_p\omega/\bar{m}^2/c_{p,s} \tag{8}$$

Equation (7) yields the following expressions for real and imaginary parts of λ as functions of frequency:

$$\lambda_{\text{real}} = 0.5\{1 + (1/\sqrt{2})[(1 + \omega_p^2)^{0.5} + 1]^{0.5}\} \tag{9a}$$

$$\lambda_{\text{imaginary}} = (1/2\sqrt{2})[(1 + \omega_p^2)^{0.5} - 1]^{0.5} \tag{9b}$$

Application of an energy balance at the surface yields a relationship between instantaneous rate of heat transfer into the solid and the instantaneous rate of heat feedback from the gas phase (S^+ represents a plane just above the surface, while S^- represents a plane just below it):

$$\left[K_g\frac{\partial T}{\partial X}\right]_{s^+} = \left[K_s\frac{\partial T}{\partial x}\right]_{s^-} - m_s Q_{\text{surf}} \tag{10}$$

(Assignment of all heat release and absorption processes in Q_{surf} to an infinitesimally thin surface region is a significant approximation.) Expansion of Eq. (10) into mean and perturbation quantities yields

$$\left[K_g\frac{\partial T'}{\partial X}\right]_{s^+} = \left[K_s\frac{\partial T'}{\partial X}\right]_{s^-} - m_s'\bar{Q}_{\text{surf}} - \bar{m}_s Q_{\text{surf}}' \tag{11}$$

where the perturbation value of surface heat release per unit mass of propellant is expressed as

$$Q_{\text{surf}}' = \left(\frac{dQ_{\text{surf}}}{dT_s}\right)T_s' \tag{12}$$

with assumption that it is a function of instantaneous surface temperature alone.

Since a critical part of this study involves allowing for differential perturbations in oxidizer and fuel ablation rates, considerable care must be taken in the calculation of m_s' and Q_{surf}' as functions of T_s'. Two limiting cases were analyzed: in scenario A (high-frequency limit), it was assumed that surface area adjustments accompanying mass flux oscillations are zero, whereas in scenario B (low-frequency limit), it was assumed that fuel and oxidizer surface areas totally compensate for the differential variations in oxidizer and fuel mass flux to maintain a constant *O/F* ratio. (In addition, parametric studies regarding intermediate frequencies were carried out via linear combinations of the limiting case expressions.) In this study, $m_s' - T_s'$ and $Q_{\text{surf}}' - T_s'$ relationships were calculated numerically via use of the steady-state model to obtain values of m_s and Q_{surf} at the mean surface temperature value and at slightly higher values (under each scenario), leading to numerical values of f_1 [defined as $(m_s'/\bar{m}_s)/T_s'$] and dQ_{surf}/dT_s.

Combining Eqs. (10–12) with $m_s'/\bar{m}_s = f_1 T_s'$ yields an expression relating perturbation values of heat flux (from the gas phase) and surface temperature:

$$q_{\text{fdbk}}' = \bar{m}c_{\text{ps}}\bar{T}_s\left[\lambda + \frac{A}{\lambda} + A\beta - \left(\frac{1}{c_{\text{ps}}}\right)\left(\frac{dQ_{\text{surf}}}{dT_s}\right)\right]\left(\frac{T_s'}{\bar{T}_s}\right) \tag{13}$$

where

$$A = f_1(\bar{T}_s - T_0), \quad \beta = -\bar{Q}_{\text{surf}}/c_{\text{ps}}(\bar{T}_s - T_0), \quad A\beta = -f_1\bar{Q}_{\text{surf}}/c_{\text{ps}}$$

Further manipulation, utilizing a mean energy balance at the surface, finally yields the desired relationship between perturbation mass burning flux and perturbation gas-phase heat-feedback flux:

$$\frac{m_s'/\bar{m}_s}{q_{\text{fdbk}}'/\bar{q}_{\text{fdbk}}} = \frac{A(1+\beta)}{\lambda + \left(\frac{A}{\lambda}\right) + A\beta - \left(\frac{1}{c_{\text{ps}}}\right)\left(\frac{dQ_{\text{surf}}}{dT_s}\right)} \tag{14}$$

Next, the gas-phase processes were analyzed for development of an additional equation relating q_{fdbk}', m_s', and P' with

Table 1 *TERM4*, *TERM5*, *A*, and maximum value of $R_{pc}^{(real)}$ for various values of AP size, pressure, and *ZFRACT*

AP diameter, μm	Pressure, atm	*ZFRACT*	*TERM-4*[a]	*A*[a]	*TERM5*[a]	Max $R_{pc}^{(r)}$
1.0	10	1.0	11.131	8.3933	+3.6953	1.22
1.0	10	0.8	10.933	8.2435	+3.0251	1.32
1.0	10	0.6	10.734	8.0937	+2.3550	1.43
1.0	10	0.4	10.535	7.9439	+1.6848	1.62
1.0	10	0.2	10.337	7.7941	+1.0146	1.84
1.0	10	0	10.138	7.6443	+0.3445	2.13
1.0	100	1.0	7.5366	6.7556	+1.6248	1.30
1.0	100	0.8	7.5641	6.7803	+1.1354	1.43
1.0	100	0.6	7.5916	6.8050	+0.6461	1.58
1.0	100	0.4	7.6192	6.8297	+0.1567	1.71
1.0	100	0.2	7.6467	6.8544	−0.3326	1.95
1.0	100	0	7.6743	6.8791	−0.8220	2.25
20.0	10	1.0	9.0925	8.3116	+4.3698	0.97
20.0	10	0.8	8.9549	8.1858	+3.7508	1.01
20.0	10	0.6	8.8174	8.0601	+3.1319	1.08
20.0	10	0.4	8.6798	7.9344	+2.5129	1.17
20.0	10	0.2	8.5423	7.8086	+1.8940	1.30
20.0	10	0	8.4047	7.6829	+1.2750	1.47
20.0	100	1.0	2.8102	7.1923	+2.8546	0.40
20.0	100	0.8	2.8221	7.2228	+2.5211	0.42
20.0	100	0.6	2.8340	7.2532	+2.1875	0.44
20.0	100	0.4	2.8459	7.2837	+1.8539	0.46
20.0	100	0.2	2.8578	7.3142	+1.5203	0.49
20.0	100	0	2.8697	7.3446	+1.1867	0.52
200.0	10	1.0	3.6739	7.5769	+1.7430	0.60
200.0	10	0.8	3.7118	7.6549	+1.4477	0.62
200.0	10	0.6	3.7497	7.7330	+1.1523	0.65
200.0	10	0.4	3.7875	7.8111	+0.8569	0.69
200.0	10	0.2	3.8254	7.8892	+0.5615	0.74
200.0	10	0	3.8633	7.9673	+0.2662	0.81
200.0	100	1.0	2.9379	8.4323	−2.5698	1.40
200.0	100	0.8	2.8828	8.2741	−2.8299	1.56
200.0	100	0.6	2.8277	8.1158	−3.0899	1.89
200.0	100	0.4	2.7725	7.9576	−3.3501	2.32
200.0	100	0.2	2.7174	7.7993	−3.6102	3.09
200.0	100	0	2.6622	7.6410	−3.8703	4.76

Note: 82/18 AP/HTPB; E_{ox} = 22,000; E_{fu} = 16,900; and K_{solid} = 0.0008 cal/cm-s-K.
[a] $R_{pc} = TERM4/(\lambda + A/\lambda + TERM5)$.

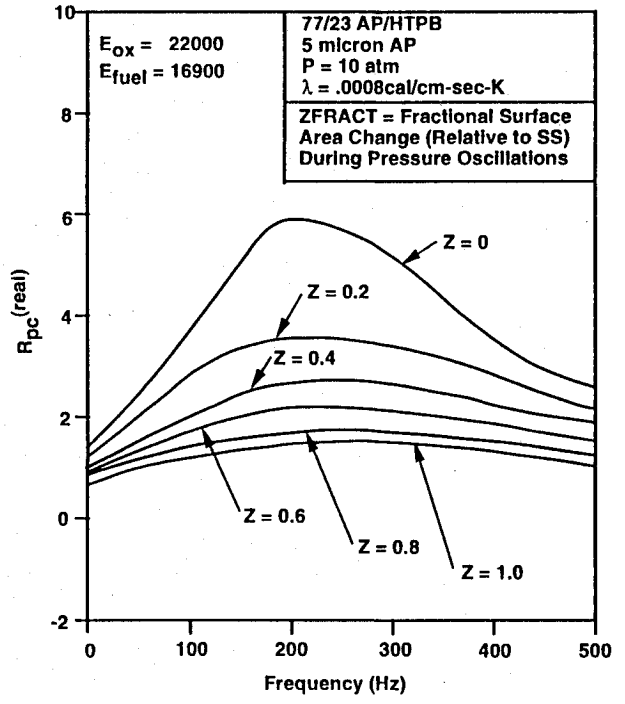

Fig. 2 Predicted $R_{pc}^{(real)}$ vs frequency curves for various values of *ZFRACT*.

this equation then being combined with Eq. (14) for elimination of q'_{fdbk}, yielding an expression for the ratio of $(m'_s/\bar{m}_s)$ to $(P'/\bar{P})$, the pressure-coupled response function. With the gas-phase analysis used, there are only three independent parameters influencing instantaneous heat-feedback flux to the propellant surface: 1) instantaneous surface temperature T_s, 2) instantaneous flame temperature T_f, and 3) instantaneous pressure P. The gas-phase processes are assumed to be quasi-steady; thus, the next step involved the calculation of partial derivatives relating perturbations in heat-feedback flux to perturbations in surface temperature, flame temperature, and pressure.

First, the surface temperature was set equal to the mean surface temperature (calculated from the steady-state model) and the quasisteady gas-phase analysis was used to calculate the gas-phase heat-feedback flux at the mean pressure and flame temperature. The surface temperature was next perturbed slightly upward, with pressure and flame temperature being held at their mean values, and new values of heat-feedback flux were calculated under both scenarios A and B. From these three calculated heat-feedback fluxes, the partial derivative of heat-feedback flux with respect to surface temperature at constant pressure and flame temperature was calculated for each scenario from

$$L \equiv \left.\frac{\partial q_{fdbk}}{\partial T_s}\right|_{T_f,P} = \frac{(q_{fdbk,\bar{T}_s+\Delta T_s,\bar{T}_f,\bar{P}} - q_{fdbk,\bar{T}_s,\bar{T}_f,\bar{P}})}{\Delta T_s} \qquad (15)$$

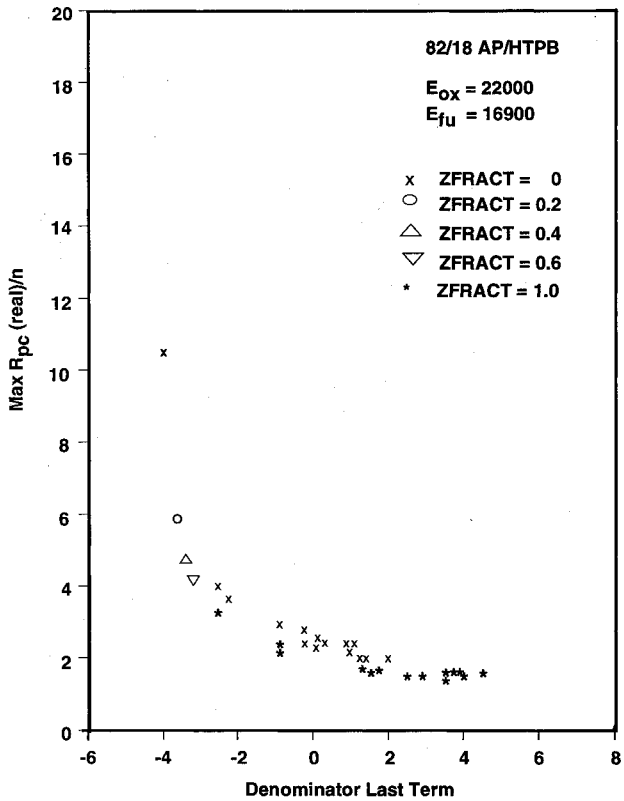

Fig. 3 Variation of maximum value of real part of pressure-coupled response function (normalized by burning rate exponent) with *TERM5* [Eq. (33)].

A similar approach was used to calculate the partial derivatives of heat-feedback flux with respect to pressure and flame temperature:

$$N \equiv \left.\frac{\partial q_{\text{fdbk}}}{\partial P}\right|_{T_s,T_f} = \frac{(q_{\text{fdbk},\bar{T}_s,\bar{T}_f,\bar{P}+\Delta P} - q_{\text{fdbk},\bar{T}_s,\bar{T}_f,\bar{P}})}{\Delta P} \tag{16}$$

$$M \equiv \left.\frac{\partial q_{\text{fdbk}}}{\partial T_f}\right|_{T_s,P} = \frac{(q_{\text{fdbk},\bar{T}_s,\bar{T}_f+\Delta T_f,\bar{P}} - q_{\text{fdbk},\bar{T}_s,\bar{T}_f,\bar{P}})}{\Delta T_f} \tag{17}$$

Using linear-superposition principles (this is a linearized analysis), perturbations in heat-feedback flux were then related to perturbations in surface temperature, flame temperature, and pressure by

$$q'_{\text{fdbk}} = LT'_s + MT'_f + NP' \tag{18}$$

At this point, we have four equations [Eqs. (12), (14), (18), and $m'_s/\bar{m}_s = f_1 T'_s$] in six perturbation quantities (T'_s, T'_f, P', m'_s, Q'_{surf}, and q'_{fdbk}) and require one more equation for the desired calculation of m'_s as a function of P'. This closure equation is derived from perturbation of the gas-phase energy balance:

$$m_s Q_{\text{gas}} = m_s c_{pg}(T_f - T_s) + q_{\text{fdbk}} \tag{19}$$

$$Q_{\text{gas}} = \Delta H_{\text{TOT}} - Q_{\text{surf}}$$

$$= f[m_{\text{ox},s} ASOX/(m_{\text{ox},s}\text{ASOX} + m_{\text{fu}} AFU)] - Q_{\text{surf}} \tag{20}$$

ΔH_{TOT} is, of course, dependent on the relative mass flow rates (mass flux-surface area products) of oxidizer and fuel leaving the surface at any time. Calculation of this available

Table 2 Pressure-coupled response function expression and maximum value of real part for various values of E_{BINDER} at constant E_{ox} and various values of E_{ox} at constant E_{BINDER}

$E_{\text{other ingredient}}$	Response function expression	Max $R_{\text{pc}}^{(\text{real})}$
	A. E_{ox} = 22,000, $ZFRACT$ = 0.0	
14,500	$R_{\text{pc}} = 9.62518/[\lambda + 7.49417/\lambda - 1.06186]$	2.89
16,900	$R_{\text{pc}} = 9.82654/[\lambda + 7.65096/\lambda + 0.50946]$	1.99
19,500	$R_{\text{pc}} = 10.0445/[\lambda + 7.82081/\lambda + 2.21404]$	1.50
22,000	$R_{\text{pc}} = 10.2536/[\lambda + 7.98413/\lambda + 3.84654]$	1.23
24,500	$R_{\text{pc}} = 10.4633/[\lambda + 8.14744/\lambda + 5.49289]$	1.04
27,000	$R_{\text{pc}} = 10.6730/[\lambda + 8.31074/\lambda + 7.14231]$	0.91
	B. E_{ox} = 22,000, $ZFRACT$ = 1.0	
14,500	$R_{\text{pc}} = 10.8926/[\lambda + 8.48100/\lambda + 3.85834]$	1.28
16,900	$R_{\text{pc}} = 10.7470/[\lambda + 8.36765/\lambda + 3.80966]$	1.28
19,500	$R_{\text{pc}} = 10.6134/[\lambda + 8.26374/\lambda + 3.76402]$	1.27
22,000	$R_{\text{pc}} = 10.5082/[\lambda + 8.18236/\lambda + 3.72875]$	1.27
24,500	$R_{\text{pc}} = 10.4272/[\lambda + 8.11935/\lambda + 3.69603]$	1.27
27,000	$R_{\text{pc}} = 10.3701/[\lambda + 8.07483/\lambda + 3.66935]$	1.27
	C. E_{BINDER} = 16,900, $ZFRACT$ = 0.0	
24,000	$R_{\text{pc}} = 10.5909/[\lambda + 8.24613/\lambda + 0.45475]$	2.11
22,000	$R_{\text{pc}} = 9.82654/[\lambda + 7.65096/\lambda + 0.50946]$	1.99
19,500	$R_{\text{pc}} = 8.87220/[\lambda + 6.90696/\lambda + 0.57543]$	1.85
16,900	$R_{\text{pc}} = 7.87791/[\lambda + 6.13323/\lambda + 0.66817]$	1.68
14,500	$R_{\text{pc}} = 6.96012/[\lambda + 5.41901/\lambda + 0.76338]$	1.52
12,000	$R_{\text{pc}} = 6.00415/[\lambda + 4.67502/\lambda + 0.87207]$	1.35
11,000	$R_{\text{pc}} = 5.62131/[\lambda + 4.37741/\lambda + 0.91831]$	1.28
	D. E_{BINDER} = 16,900, $ZFRACT$ = 1.0	
24,000	$R_{\text{pc}} = 11.8575/[\lambda + 9.23228/\lambda + 5.05341]$	1.20
22,000	$R_{\text{pc}} = 10.7470/[\lambda + 8.36765/\lambda + 3.80996]$	1.28
19,500	$R_{\text{pc}} = 9.41003/[\lambda + 7.32566/\lambda + 2.24120]$	1.43
16,900	$R_{\text{pc}} = 8.02986/[\lambda + 6.25152/\lambda + 0.59830]$	1.73
14,500	$R_{\text{pc}} = 6.78779/[\lambda + 5.28484/\lambda - 0.92930]$	2.39
12,000	$R_{\text{pc}} = 5.52511/[\lambda + 4.30202/\lambda - 2.52811]$	5.90
11,000	$R_{\text{pc}} = 5.03852/[\lambda + 3.92358/\lambda - 3.17608]$	≈31

Note: 82/18 AP/HTPB, 7-μm AP, and pressure = 10 atm.

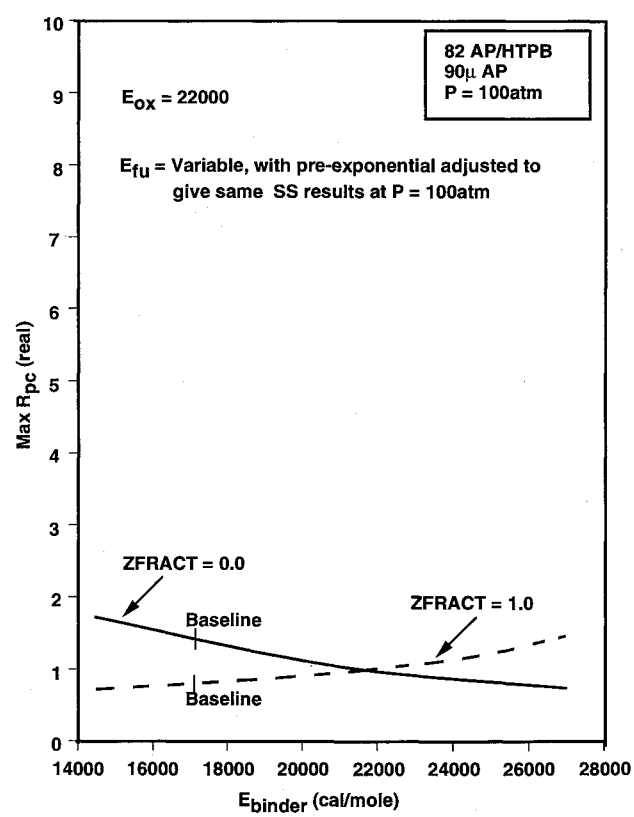

Fig. 4 Dependence of maximum value of $R_{\text{pc}}^{(\text{real})}$ on binder ablation activation energy.

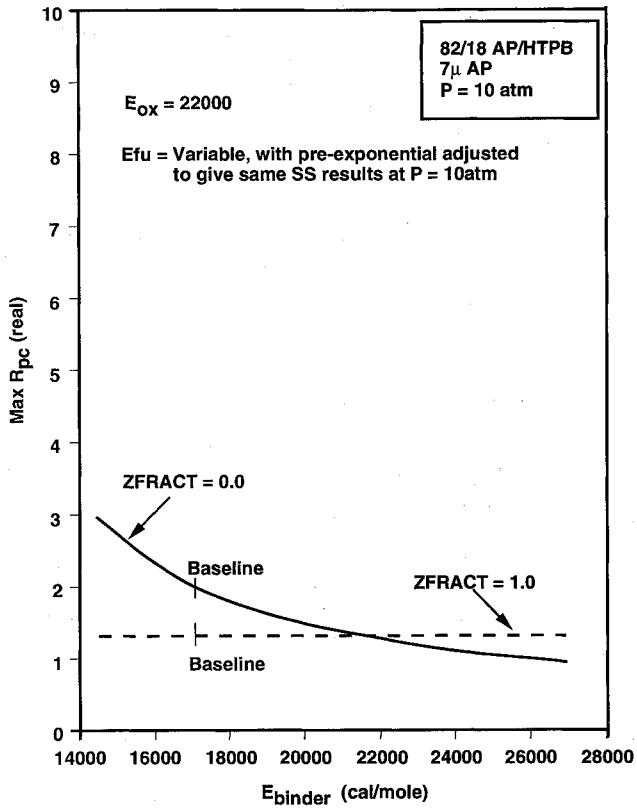

Fig. 5 Dependence of maximum value of $R_{pc}^{(real)}$ on binder ablation activation energy.

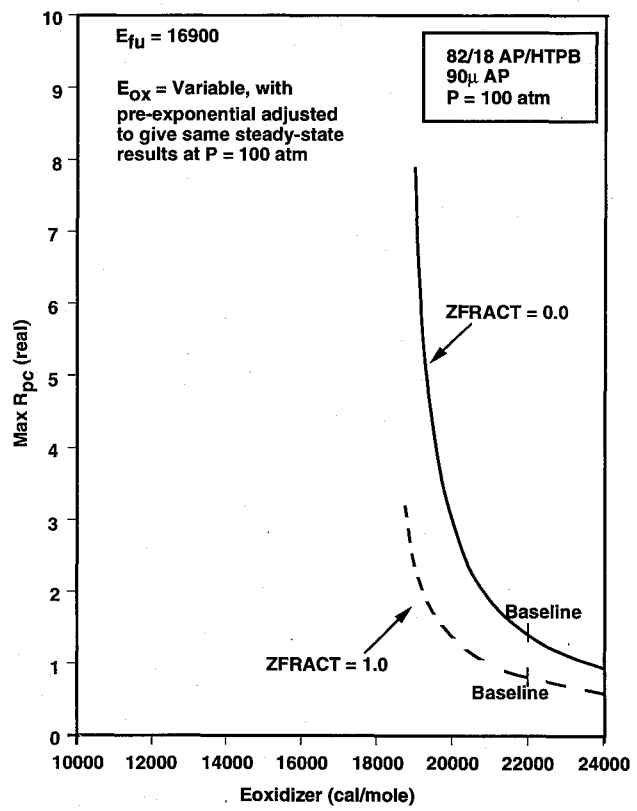

Fig. 6 Dependence of maximum value of $R_{pc}^{(real)}$ on oxidizer ablation activation energy.

energy as a function of oxidizer/fuel ratio over a range of interest for practical propellant compositions yields

$$\Delta H_{TOT} = -2050 + 3600[m_{ox,s}ASOX/(m_{ox,s}ASOX + m_{fu}AFU)] \tag{21}$$

where the quantity inside the brackets is a function of the surface temperature, with this functionality differing under scenarios A and B. With use of linearized analysis and definition of the quantity relating perturbations in the bracketed term to perturbations in surface temperature as

$$f_3 = [\,]'/T_s' \tag{22}$$

it can be readily shown that under scenario B, $f_3 = 0$, whereas under scenario A,

$$f_3 = (\{A_{ox} \exp[-E_{ox}/R(\bar{T}_s + T_s')]\overline{ASOX}/\{A_{ox} \exp[-E_{ox}/R(\bar{T}_s + T_s')]\overline{ASOX} + A_{fu} \exp[-E_{fu}/R(\bar{T}_s + T_s')]\overline{AFU}\}\} - \mathrm{WFO})/T_s' \tag{23}$$

Perturbation of Eq. (21), with the substitution of Eq. (22) then yields

$$\Delta H_{TOT}' = 3600 f_3 T_s' \tag{24}$$

with subsequent perturbation of Eq. (20) yielding

$$Q_{gas}' = 3600 f_3 T_s' - \left(\frac{dQ_{surf}}{dT_s}\right) T_s' = f_4 T_s' \tag{25}$$

Expansion of Eq. (19) into steady-state and perturbation quantities next yields,

$$q_{fdbk}' = m_s' \bar{q}_{fdbk}/\bar{m}_s + \bar{m}_s Q_{gas}' - \bar{m}_s c_{pg}(T_f' - T_s') \tag{26}$$

which, in conjunction with Eq. (25), provides the final closure equation. At this point, we have six equations [Eqs. (12), (14), (18), (25), (26), and $m_s'/\bar{m}_s = f_1 T_s'$] in seven unknown quantities (q_{fdbk}', T_s', T_f', P', m_s', Q_{surf}', and Q_{gas}'); these yield the desired expression for R_{pc}:

$$R_{pc} \equiv \frac{m_s'/\bar{m}_s}{P'/\bar{P}} = N/\{[M/\bar{m}_s c_{pg} + 1][\lambda + A/\lambda + A\beta - (1/c_{ps})(dQ_{surf}/dT_s)][\bar{q}_{fdbk}]/[A(1+\beta)\bar{P}] - M\bar{q}_{fdbk}/\bar{m}_s/c_{pg}/\bar{P} - (f_4/c_{pg}f_1 + L/f_1 M + 1/f_1)M/\bar{P}\} \tag{27}$$

where procedures for calculation of A, B, L, M, N, dQ_{surf}/dT_s, f_1, and f_4 under either limiting scenario as regards surface topology adjustment have been discussed, and $\bar{q}_{fdbk}$ and $\bar{m}_s$ are available from the steady-state model. The real part of the pressure-coupled response is calculated for various frequencies using the following procedure. First, the frequency is substituted into Eq. (8) for calculation of dimensionless angular frequency. Equations (9a) and (9b) are then used to calculate real and imaginary parts of λ, which are then substituted into Eq. (27) for calculation of real and imaginary parts of R_{pc}.

As indicated earlier, two limiting case scenarios as regards surface topology adjustments during pressure oscillations were treated in the equation development for f_1 (appearing in the constant A), f_4, dQ_{surf}/dT_s, and L; in the following studies, allowance was made for partial surface area adjustments through the use of a parameter, *ZFRACT* (0.0 for scenario A and 1.0 for scenario B), with the values of each of the quantities that are scenario-dependent being calculated as

$$X_j = (1 - ZFRACT)X_{j,\text{scenario A}} + ZFRACT X_{j,\text{scenario B}} \tag{28}$$

In the first phase, *ZFRACT* was treated simply as a model input, with effects on calculated response function vs fre-

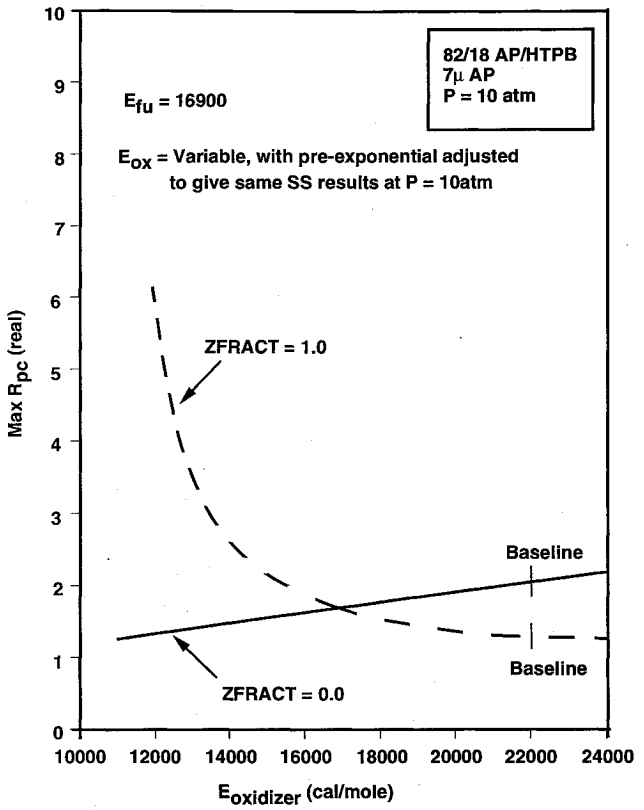

Fig. 7 Dependence of maximum value of $R_{pc}^{(real)}$ on oxidizer ablation activation energy.

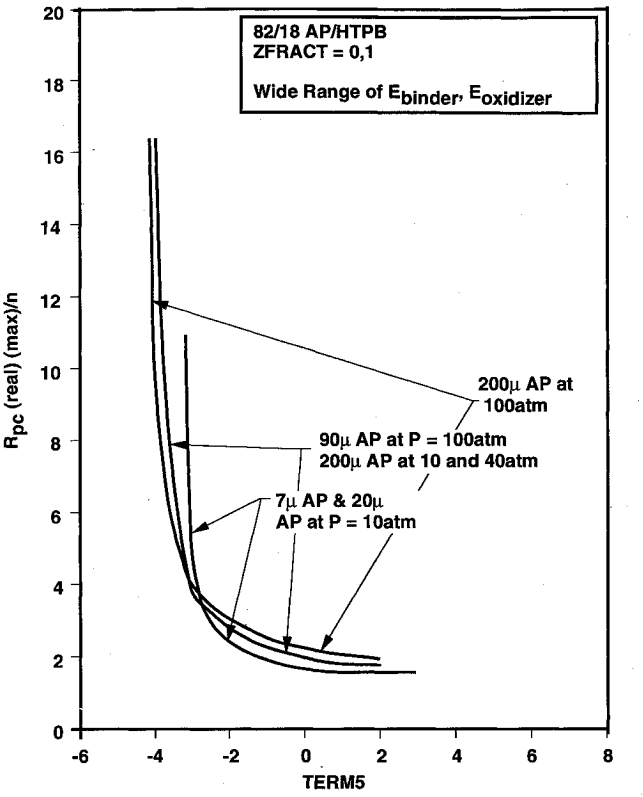

Fig. 8 Dependence of maximum values of $R_{pc}^{(real)}$ divided by burning rate exponent on *TERM5* for several pressure-particle size combinations.

quency curves being examined parametrically. In the second phase, an expression was used relating *ZFRACT* to the ratio of the characteristic oscillation time and the time to burn a thickness of propellant equal to one oxidizer diameter. This time ratio, *TIMRAT*, was calculated as

$$TIMRAT = \bar{m}/f\rho_{prop}D_{ox} \tag{29}$$

Included in user inputs to the computer code utilized in this study was a value of *TIMRAT* above which *ZFRACT* = 1.0 (*TRATMX*) and a value of *TIMRAT* below which *ZFRACT* = 0.0 (*TRATMN*); between these limits, it was assumed that *ZFRACT* could be related to *TIMRAT* by an expression of the form

$$ZFRACT = K_1 + K_2\,\ell n(TIMRAT) \tag{30}$$

where K_1 and K_2 were calculated using *ZFRACT* = 1.0 at *TIMRAT* = *TRATMX* and *ZFRACT* = 0.0 at *TIMRAT* = *TRATMN*, leading to

$$K_2 = 1.0/[\ell n(TRATMX) - \ell n(TRATMN)] \tag{31}$$

$$K_1 = -K_2\,\ell n(TRATMN) \tag{32}$$

Results of Parametric Studies

In the first part of the study, where ZFRACT was treated parametrically, with results being calculated for various user-input values of this parameter (held constant over the frequency range studied), a closed-form expression for the pressure-coupled response is obtained:

$$R_{pc} = TERM4/(\lambda + A/\lambda + TERM5) \tag{33}$$

where *TERM4*, *TERM5*, and *A* are independent of frequency for a given propellant and mean pressure. {Note the similarity with typical homogeneous propellant response functions of the form $R_{pc} = nAB/[\lambda + A/\lambda - (1 + A) + A\beta]$, with, however, major differences in *TERM4* and *TERM5*, which are not equal to *nAB* and $[A\beta - (1 + A)]$ in this heterogeneous propellant model.} In the second phase of the study, where *ZFRACT* was calculated as a function of the ratio of oscillation time to the time required for burning of one oxidizer-diameter thickness, *ZFRACT* is a function of the oscillation frequency; in this case, such a closed-form expression cannot be obtained.

Variant I—Input Values of *ZFRACT*

Calculations were first performed for baseline values of the ingredient ablation activation energies, 22,000 cal/mole for AP and 16,900 cal/mole for the binder. Typical plots of the real part of the pressure-coupled response are plotted against frequency in Fig. 2. As may be seen, predicted magnitudes of the real parts of the response function decrease significantly with increasing values of *ZFRACT*; i.e., surface area variation compensation for differential sensitivity of oxidizer and fuel ablation to surface temperature variations results in considerable stabilization.

Values of *TERM4*, *TERM5*, and *A* [Eq. (33)], along with maximum values of the real part of R_{pc} are tabulated in Table 1 for 82/18 AP/HTPB formulations for various pressure-AP particle size combinations. (Similar tables were generated for additional combinations and appear in Ref. 11.) Again, it is seen that the maximum value of the real part of the pressure-coupled response function decreases significantly as more surface area adjustment is allowed (larger *ZFRACT*). The maximum value of the real part of R_{pc}, normalized by the steady-state burning rate exponent *n*, correlates well with *TERM5* values, decreasing as *TERM5* increases (see Fig. 3). It is of interest to examine *TERM5* further to see what factors lead to increased values and to the decrease in the real part of the response function.

Comparison of Eqs. (27) and (33) yields an expression relating *TERM5* to various parameters:

$$TERM5 = \frac{-A\bar{Q}_{surf}}{c_{ps}(\bar{T}_s - T_0)} - \frac{dQ_{surf}/dT_s}{c_{ps}} - \frac{M(\bar{T}_s - T_0)(\bar{q}_{fdbk}f_1/\bar{m}_s/c_{p,gas} + f_4/c_{p,gas} + L/M + 1.0)(1.0 - Q_{surf}/c_{ps}/(\bar{T}_s - T_0))}{\bar{q}_{fdbk}/(M/\bar{m}_s/c_{p,gas} + 1.0)} \quad (34)$$

As seen, decreases in dQ_{surf}/dT_s (more negative), f_4 (less positive), and L (less positive or more negative) all lead to increases in *TERM5* and to decreases in maximum $R_{pc}^{(real)}/n$; examination of detailed code outputs indicates that decreases in these parameters accompany increases in *ZFRACT*. Changes in L and dQ_{surf}/dT_s with *ZFRACT* affect *TERM5* roughly equally, while changes in f_4 are dominant for small AP particle size cases, but much less important for large AP cases. Noting that $f_4 = dQ_{gas}/dT_s$ and $L = \partial q_{fdbk}/\partial T_s$ (at constant flame temperature and pressure), we see that increases in *ZFRACT* lead to decreases in maximum $R_{pc}^{(real)}/n$ values (accompanying increases in *TERM5*) by causing decreases in the partial derivative of heat-feedback flux with respect to surface temperature. These *ZFRACT* increases also lead to decreases in the derivative of gas-plus-surface heat release with respect to surface temperature (leading to decreases in the derivative of flame temperature with respect to surface temperature, also leading to lower increases in heat-feedback flux for a given increase in surface temperature).

Effects of changes in the activation energies of ablation of oxidizer and fuel were next examined for limiting *ZFRACT* = 0 and *ZFRACT* = 1 cases. In one set of calculations, the activation energy of the oxidizer ablation process was held at its baseline value of 22,000 cal/mole with the activation energy of the fuel being varied; in a second set of calculations, the fuel ablation activation energy was held at its baseline value of 16,900 cal/mole, while the oxidizer ablation activation energy was varied. In all cases, for either ingredient, the preexponential in the ablation rate expression was adjusted to keep the steady-state burning rate at the prescribed pressure constant as the activation energy varied. Tabular results in the form of R_{pc} expressions and maximum $R_{pc}^{(real)}$ values vs binder ablation activation energy at E_{ox} = 22,000, and vs oxidizer activation energy at E_{fuel} = 16,900, are presented for one formulation in Table 2; further results appear in Appendix A of Ref. 11.

Maximum values of $R_{pc}^{(real)}$ are plotted against activation energy of binder ablation at a fixed value of oxidizer ablation activation energy (22,000 cal/mole) for two pressure-particle size combinations for *ZFRACT* = 0 and *ZFRACT* = 1 in Figs. 4 and 5. Figures 6 and 7 show similar plots of maximum $R_{pc}^{(real)}$ vs oxidizer ablation activation energy for the baseline fuel ablation activation energy of 16,900 cal/mole. As may be seen, for *ZFRACT* = 0, the maximum $R_{pc}^{(real)}$ values decrease monotonically with increasing E_{BINDER}. However, even for the no-surface-topology-adjustment cases, the predicted effects of varying $E_{OXIDIZER}$ at constant E_{BINDER} are not so simple; for the 90-μm AP cases, the maximum $R_{pc}^{(real)}$ values decrease with increasing $E_{OXIDIZER}$, whereas for the 7-μm AP case the maximum $R_{pc}^{(real)}$ values increase with increasing $E_{OXIDIZER}$. With complete surface area adjustment during oscillations, the maximum value of $R_{pc}^{(real)}$ either increases or remains constant (depending on oxidizer size and pressure) with increasing binder ablation activation energy at constant $E_{OXIDIZER}$, while it decreases with increasing oxidizer ablation activation energy at fixed E_{BINDER}.

As with the baseline cases, maxima in the $R_{pc}^{(real)}$ vs frequency curves were found to correlate well with *TERM5* in the response function equation [Eq. (33)] over the entire range of activation energies and *ZFRACT* values examined for each

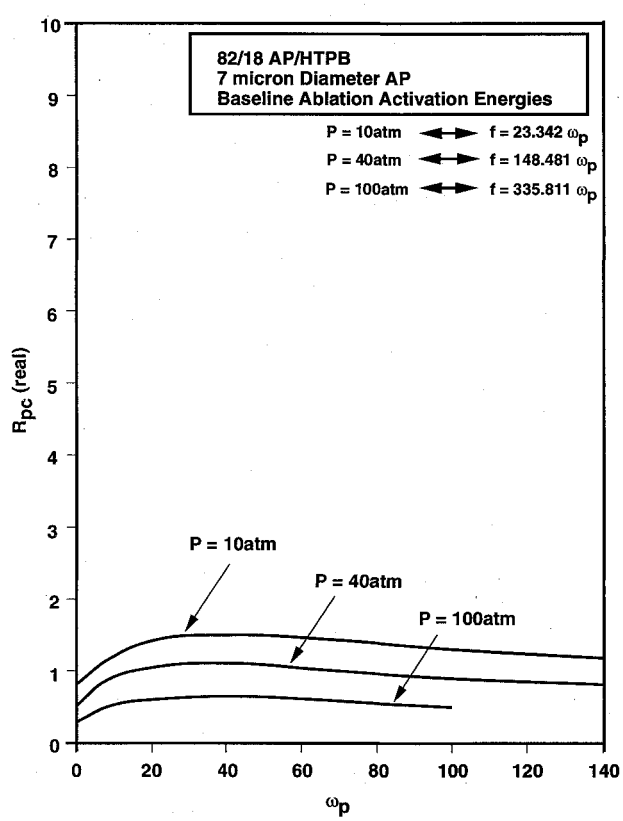

Fig. 9 Real part of pressure-coupled response vs dimensionless frequency, 7-μm AP.

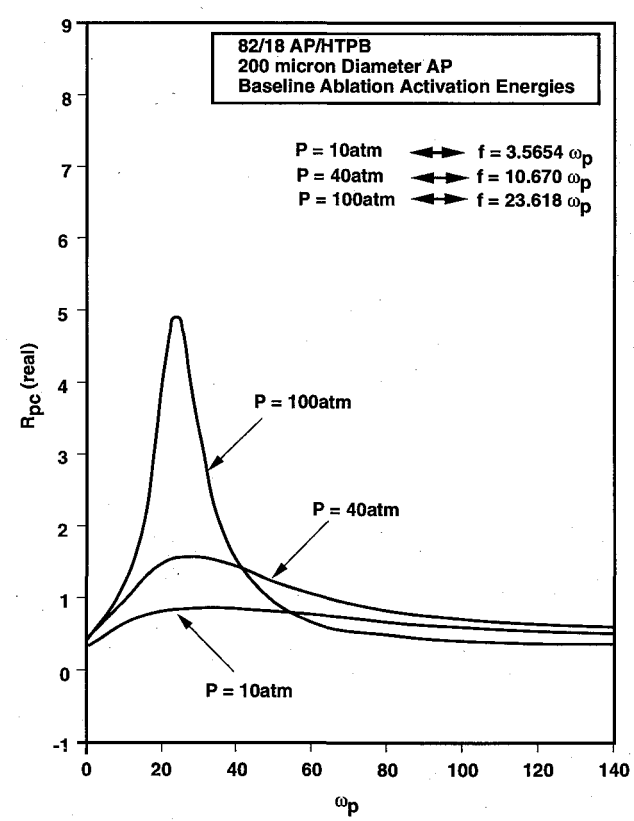

Fig. 10 Real part of pressure-coupled response vs dimensionless frequency, 200-μm AP.

pressure-particle size combination, with these maximum values decreasing with increasing values of *TERM5*. Normalization of these maximum values by the burning-rate exponents yields similarly good correlation with *TERM5*, as shown in Fig. 8.

Identification of factors leading to changes in *TERM5* [and in maximum values of $R_{pc}^{(real)}$] with changes in $E_{OXIDIZER}$ (at fixed E_{BINDER}) and changes in E_{BINDER} (at fixed $E_{OXIDIZER}$) is of interest. Examination of detailed computer outputs indicates that several factors contribute significantly to changes in *TERM5* with changes in $E_{OXIDIZER}$ and E_{BINDER} (all other parameters being held constant); the relative importance of these factors was seen to vary from case-to-case, preventing useful generalizations (see Ref. 11 for more detail).

Variant II—Calculations with *ZFRACT* Being a Function of a Characteristic Oscillation Time/Burn Time Ratio

As with the studies involving input values of *ZFRACT*, discussions of studies using an expression relating *ZFRACT* to the ratio of oscillation time to time to burn through a thickness of propellant equal to one oxidizer particle diameter are broken into two parts. These parts are calculations with baseline values of oxidizer and fuel ablation activation energies and those using various values of these activation energies. The following relationship between *ZFRACT* and *TIMRAT* was utilized (other expressions could obviously be used in further studies, but should not change conclusions in any major way):

$$\begin{aligned} ZFRACT &= 0.0 \quad \text{for} \quad TIMRAT < 0.1 \\ ZFRACT &= [\ell n(TIMRAT) - \ell n(0.1)] \\ &/[\ell n(10) - \ell n(0.1)] \quad \text{for} \quad 0.1 < TIMRAT < 10 \\ ZFRACT &= 1.0 \quad \text{for} \quad TIMRAT > 10.0 \end{aligned} \tag{35}$$

For baseline activation energies for oxidizer and binder ablation, plots of predicted values of $R_{pc}^{(real)}$ vs ω_p are presented in Figs. 9 and 10 (for pressures of 10, 40, and 100 atm) for two 82/18 AP/binder formulations with different AP particle

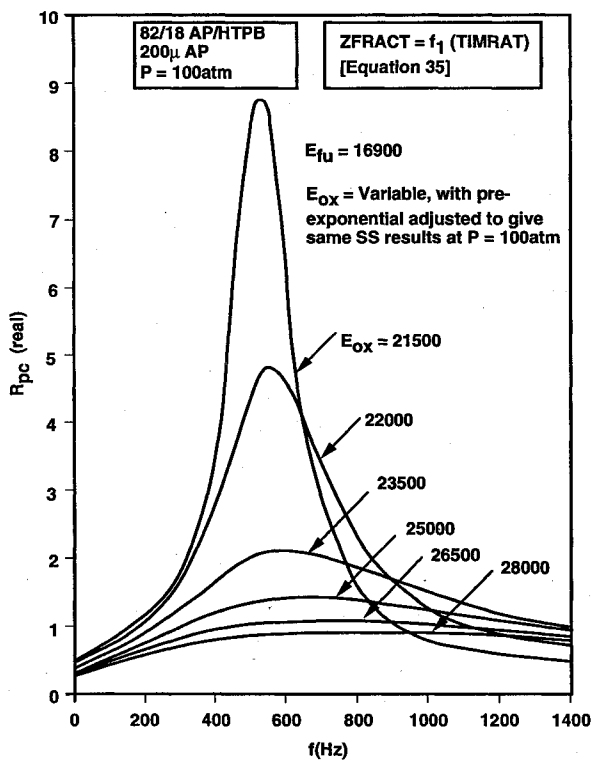

Fig. 11 $R_{pc}^{(real)}$ vs oscillation frequency for various values of E_{ox} at E_{fuel} = 16,900 cal/mole, 200-μm AP, P = 100 atm.

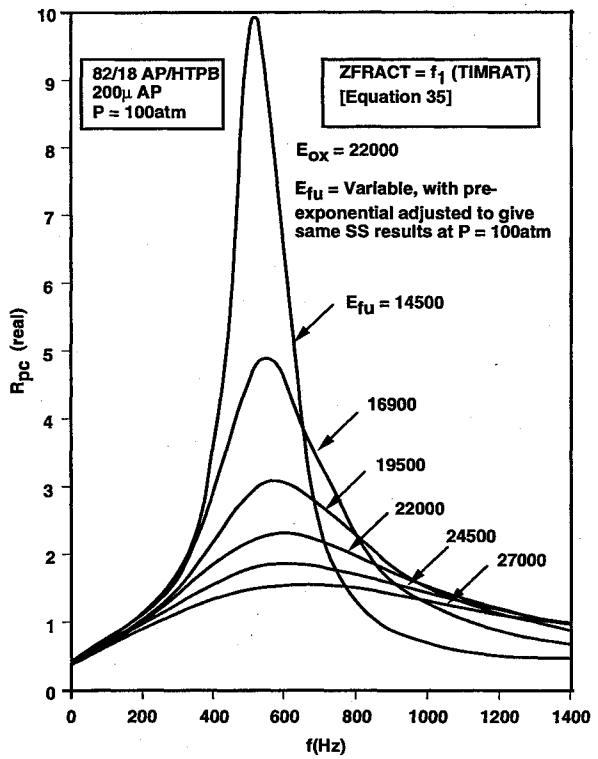

Fig. 12 $R_{pc}^{(real)}$ vs oscillation frequency for various values of E_{fuel} at E_{ox} = 22,000 cal/mole, 200-μm AP, P = 100 atm.

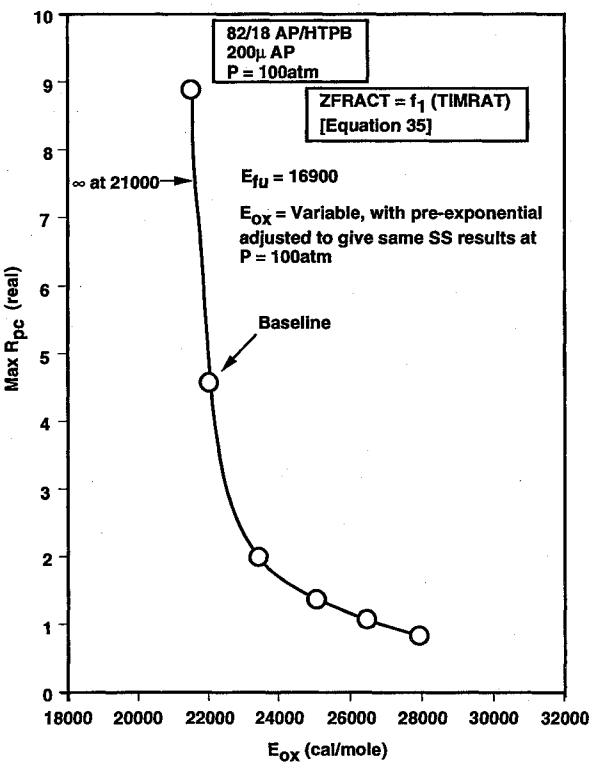

Fig. 13 Dependence of maximum value of $R_{pc}^{(real)}$ on E_{ox} at E_{fuel} = 16,900 cal/mole, 200-μm AP, P = 100 atm.

sizes. Since *ZFRACT* decreases (less surface area adjustment) with increasing frequency, these curves in most cases have somewhat different shapes than the curves of Fig. 2, where *ZFRACT* was held constant for each curve. At the lowest frequencies, the response values correspond to *ZFRACT* = 1.0 values on the earlier figure, while at the highest frequencies, they are closer to the *ZFRACT* = 0 values. As may be seen

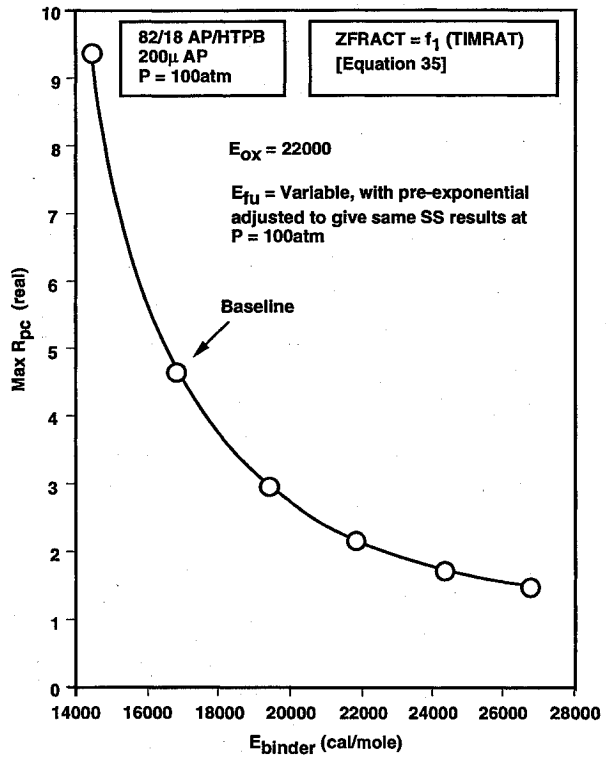

Fig. 14 Dependence of maximum value of $R_{pc}^{(real)}$ on E_{fuel} at E_{ox} = 22,000 cal/mole, 200-μm AP, P = 100 atm.

from these figures, the pressure-coupled responses for the smaller AP cases are fairly low, without any sharp peaks, but as the AP size is increased, the pressure-coupled response vs dimensionless frequency curves exhibit significant peaks, particularly at high pressure.

Plots of calculated $R_{pc}^{(real)}$ vs oscillation frequency are presented in Figs. 11 and 12 for various values of oxidizer ablation activation energy (at constant fuel ablation activation energy) and various values of fuel ablation activation energy (at constant oxidizer ablation activation energy) for one pressure-oxidizer particle size combination. (Again, considerably more results are presented in Ref. 11.) The maximum values of this real part of the pressure-coupled response, extracted from these and additional plots, are next plotted against oxidizer ablation activation energy for one pressure-AP size combination in Fig. 13, and against fuel ablation activation energy in Fig. 14.

As may be seen from Fig. 13, the maximum value of $R_{pc}^{(real)}$ decreases with increasing value of the oxidizer ablation activation energy (at fixed fuel ablation activation energy). This result is opposite of predictions made with the preliminary model[3-5] discussed earlier; in that preliminary model it should be recalled that the pressure-coupled response real parts were predicted to increase with increasing oxidizer ablation activation energy at fixed binder ablation activation energy. Careful examination of the computer printouts indicates that this change comes about as a result of treatment of the condensed-phase heat dependency on various parameters in the current modeling effort; this factor appears to more than compensate for the effects of the relative ablation activation energies on the degree of oscillation of oxidizer/fuel ratio of gas packets leaving the propellant surface. (These latter effects tend to lead to lower response of burning rate to pressure oscillations with decreased values of $E_{OXIDIZER} - E_{BINDER}$.)

Figure 14 shows that predicted maxima in $R_{pc}^{(real)}$ decrease with increasing values of E_{BINDER} (at fixed $E_{OXIDIZER}$) for all cases examined, in qualitative agreement with the preliminary studies of Refs. 3–5. However, the magnitude of these decreases is less than predicted in the preliminary studies.

Summary/Conclusions

The effects of different activation energies of oxidizer and fuel ablation on the pressure-coupled response functions of AP-composite propellants have been examined using a perturbation analysis applied to a complex steady-state composite propellant burning rate model. Two limiting cases have been examined: one for low-frequency oscillations where surface areas of oxidizer and fuel adjust to mass flux oscillations of these species to keep the oxidizer/fuel ratio of evolving gases constant and the other for high-frequency oscillations where there is no such compensation. In addition, intermediate cases have been studied with ratio of oscillation time to characteristic burning time being used to characterize the degree of area adjustment as a function of oscillation frequency, permitting development of curves of the real part of the response function vs frequency with allowance for the fact that the degree of area ratio adjustment will vary from total at zero frequency to zero at high frequency. From limited calculations to date, it is seen that either increasing oxidizer ablation activation energy at fixed binder activation energy or increasing binder ablation activation energy at a fixed oxidizer ablation activation energy can result in significant reduction of the pressure-coupled burning rate response.

Acknowledgments

The support of the Air Force Office of Scientific Research with Mitat Birkan as Program Manager, under Contract F49620-90-C-0067, is gratefully acknowledged. Consultation and advice provided by R. H. W. Waesche on this project is also greatly appreciated.

References

[1]Culick, F. E. C., "Combustion Instability in Solid Rocket Motors, Vol. II: A Guide for Motor Designers," CPIA Publication 290, Laurel, MD, Jan. 1981.

[2]Summerfield, M., Caveny, L. H., Battista, R., Kubota, N., Gostintsev, Y. A., and Isoda, H., "Theory of Dynamic Extinguishment of Solid Propellants with Special Reference to Non-Steady Heat Feedback Law," *Journal of Spacecraft and Rockets*, Vol. 8, No. 3, 1971, pp. 251–258.

[3]King, M. K., "Composite Propellant Combustion Modeling: Pressure-Coupled Response Functions," AIAA Paper 80-1124, July 1980.

[4]King, M. K., "Examination of Alternate Approaches for Utilizing Steady-State Propellant Combustion Model Parameters in Calculation of Pressure-Coupled Response Functions," *18th JANNAF Combustion Meeting* (Pasadena, CA), CPIA Publication 347, Vol. III, 1981, pp. 21–29.

[5]King, M. K., "Modeling of Pressure-Coupled Response Functions of Solid Propellants," *19th International Symposium on Combustion* (Haifa, Israel), 1982, The Combustion Inst., Pittsburgh, PA, 1982, pp. 707–715.

[6]King, M. K., "Model for Steady-State Combustion of Unimodal Composite Solid Propellants," AIAA Paper 78-216, Jan. 1978.

[7]King, M. K., "A Model of the Effects of Pressure and Crossflow Velocity on Composite Propellant Burning Rate," AIAA Paper 79-1171, June 1979.

[8]King, M. K., "Experimental and Theoretical Study of the Effects of Pressure and Crossflow on Composite Propellant Burning Rate," *18th International Symposium on Combustion* (Waterloo, Canada), The Combustion Inst., Pittsburgh, PA, 1981, pp. 207–216.

[9]King, M. K., "Predicted and Measured Effects of Pressure and Crossflow Velocity on Composite Propellant Burning Rate," *17th JANNAF Combustion Meeting* (Langley, VA), Vol. 1, CPIA Publication 329, 1980, pp. 99–122.

[10]Beckstead, M. W., Derr, R. L., and Price, C. F., "The Combustion of Solid Monopropellants and Composite Propellants," *13th International Symposium on Combustion,* The Combustion Inst., Pittsburgh, PA, 1971, pp. 1047–1056.

[11]King, M. K., and Waesche, R. H. W., "Examination of Chemical Approaches to Stabilizing Composite Propellant Combustion," Final Rept. TR-PL-13278, U.S. Air Force Office of Scientific Research Contract F49620-90-C-0067, Oct. 1991.